https://doi.org/10.5194/egusphere-2026-4786
Preprint. Discussion started: 13 August 2026

Tight physics and chemistry coupling improves air quality forecasts: a case study of the 2020 North American wildfires with the Rapid Refresh model coupled to Chemistry (RAP-Chem v1.0)

Jordan Schnell[1,2], Ravan Ahmadov[2], Georg A. Grell[2], Joseph B. Olson[2], Eric James[2], Ming Hu[2], Ka Yee Wong[2,4], Brian McDonald[3], Rebecca H. Schwantes[3], Jian He[1,3], Colin Harkins[1,3], Wayne M. Angevine[1,3], Brian Jamison[2,4], R. Bradley Pierce[5], Matthew Coggon[3], Barry Baker[6], Saulo Freitas[7], Gabriel Pereira[8], Marina Tsidulko[9]

[1]Cooperative Institute for Research in Environmental Sciences (CIRES), University of Colorado Boulder, USA

[2]NOAA Global Systems Laboratory, 325 Broadway, Boulder, CO, USA

[3]NOAA Chemical Sciences Laboratory, 325 Broadway, Boulder, CO, USA

[4]Cooperative Institute for Research in the Atmosphere (CIRA), Colorado State University, 3925A West Laporte Ave, Fort Collins, CO 80521, USA

[5]Space Science and Engineering Center, University of Wisconsin-Madison, 1225 W. Dayton St., Madison, WI 53706, USA

[6]NOAA Air Resources Laboratory, 5830 University Research Court, College Park, MD 20740, USA

[7]National Institute for Space Research (INPE), Avenida dos Astronautas, 1.758, Jardim Granja - CEP 12227-010, São José dos Campos, SP - Brazil

[8]Federal University of São João del-Rei (UFSJ), Praça Frei Orlando, 170 - Centro, São João del-Rei - MG, 36307-352, Brazil

[9]NOAA National Environmental Satellite. Data, and Information Service (NESDIS), 1335 East-West Highway, SSMC1, 8th Floor, Suite 8300, Silver Spring, MD 20910, USA

Correspondence to: Jordan Schnell (jordan.schnell@colorado.edu)

https://doi.org/10.5194/egusphere-2026-4786
Preprint. Discussion started: 13 August 2026

Abstract

The Rapid Refresh model coupled to Chemistry (RAP-Chem) is an experimental forecast model built and operated by the NOAA Global Systems Laboratory (GSL). The RAP-Chem is a full chemistry extension to the operational smoke forecasting model, RAP-Smoke. RAP-Chem's chemistry includes a reduced complexity, carbon-bond, gas-phase mechanism and an aerosol scheme that are coupled together to produce secondary aerosols and perform heterogeneous chemistry. The model includes chemical lateral boundary conditions, hourly anthropogenic emissions and online emissions from biomass burning, dust, sea salt, and biogenic sources. RAP-Chem also includes the direct aerosol effect on radiation and photolysis and a simplified indirect aerosol effect that couples prognostic aerosols to representative aerosols in the aerosol-aware microphysics scheme. The default 'offline' vertical mixing implemented in WRF-Chem is updated to instead mix chemical species alongside other scalars in the model's planetary boundary layer (PBL) scheme, which tends to improve predictions across species - increasing surface ozone (O_3) and decreasing less reactive tracers (e.g., CO). Sub-grid boundary layer clouds in the PBL scheme are also coupled to a WRF-Chem photolysis scheme for the first time, overall reducing O_3 biases in the eastern US. Here we present the ability of the RAP-Chem model to simulate the extreme North American wildfires in 2020. We demonstrate that the relatively simple gas-phase chemical mechanism alongside our model physics developments and coupling with chemistry can predict maximum daily 8-h average O_3 with exceptional skill (Normalized Mean Bias (NMB) = 6.6%) averaged over CONUS, improving on simulations that neglect the direct aerosol effect (NMB = 9.5%). Ozone biases are large in regions with extreme aerosol loading, but the NMB improves more significantly. The model produces the observed extreme aerosol loading with less skill; tending to underpredict extreme wildfire induced concentrations while overpredicting urban particle pollution. As with O_3, daily average $PM_{2.5}$ is predicted with better skill when the direct aerosol feedback is included (-15.8% vs. -16.8%). Overall we find that improving the coupling between chemistry and physics processes in the air quality model improves its predictions of both weather and atmospheric composition.

1 Introduction

Timely and accurate air quality forecasts are essential tools to protect public health, particularly in areas heavily influenced by urban and/or wildfire emissions. The Rapid Refresh assimilation and forecasting model (RAP-Smoke; Benjamin et al., 2016) is an hourly-updating system that has been providing operational predictions of meteorology and wildfire smoke at NOAA since December, 2020. The RAP-Smoke is built off of the Weather Research and Forecasting model (WRF; (Skamarock et al., 2008; Powers et al., 2017) with the Advanced Research WRF (ARW) dynamical core, with smoke emissions and plume rise parameterizations built off of the WRF coupled to chemistry (i.e., WRF-Chem; Grell et al., 2005). WRF-Chem is the air quality component of WRF and contains a range of emission source schemes, chemical mechanisms, and feedbacks to physics. Experimental forecasts were produced with RAP-Smoke at the NOAA Global Systems Laboratory (GSL) during its development, and, as an experimental follow-on to this project, we have coupled additional WRF-Chem chemistry packages to the RAP in an effort to build a more comprehensive air quality modeling system described herein.

https://doi.org/10.5194/egusphere-2026-4786
Preprint. Discussion started: 13 August 2026

WRF-Chem is considered a "fully coupled" air quality model in that air composition is allowed to provide a forcing on forecasted meteorology (Grell et al., 2005). Additionally, the chemical and meteorological tracers of WRF-Chem share the same grid and advection schemes, and optionally the same time step. This differs from an "offline" model where the meteorological forcing is obtained through a meteorology-only simulation prior to the chemical simulation. Moreover, the meteorology only simulation need not be on the same grid as the subsequent chemistry simulation (i.e., the meteorological fields are interpolated in both time and space). Indeed, the RAP/HRRR-Smoke system includes the direct aerosol effect by including extinction due to smoke in its radiation module (Benjamin et al., 2016). However, RAP/HRRR-Smoke only simulates a single smoke aerosol tracer, and so the aerosol feedback is routinely underestimated due to other missing aerosol sources (e.g., anthropogenic activities, dust, etc.), which likely contributes to the bias in HRRR (James et al., 2022). Moreover, the impact of aerosols on radiation is calculated via a look-up-table approach as opposed to a physically-based calculation of extinction (e.g., Mie theory) that can take into account aerosol size and mixing state.

While WRF-Chem is considered "fully-coupled", there are still inconsistencies between physics and chemistry. For example, with the exception of the ACM2 planetary boundary layer (PBL) scheme (Pleim, 2007), the vertical mixing of meteorological tracers in WRF-Chem is handled separately from the vertical mixing of chemical tracers. Instead, an exchange coefficient is diagnosed in the PBL scheme and passed to a separate dedicated vertical mixing routine in the chemistry code, which only performs *local* mixing (i.e., only mixing between adjacent layers). Thus if a user selects a non-local PBL scheme, the vertical mixing of meteorological and chemical tracers will be inconsistent. The RAP/HRRR-Smoke system uses the Mellor–Yamada–Nakanishi–Niino with eddy-diffusivity / mass-flux (MYNN-EDMF) adapted from Nakanishi & Niino (2004, 2009), which like ACM2 can now also mix all chemical species both locally and nonlocally. The MYNN-EDMF scheme produces its own subgrid cloud macrophysics, separate from the microphysics and cumulus parameterizations. These clouds were initially coupled to the RRTMG radiation schemes (Benjamin et al. 2016, Olson et al. 2026), but they were not added to the photolysis schemes in WRF-Chem (i.e., those schemes that calculate the disassociation of molecules due to sunlight). Thus, the meteorological parameterizations would receive different actinic fluxes than those in chemistry. A similar situation exists for the cumulus parameterization: until WRF-Chem v4.3 (released May 2021), convective transport of chemical tracers could only be performed by a version of the Grell-Devyani cumulus scheme (Grell & Dévényi, 2002) embedded into the chemistry code. Accordingly, unless the user also chose to use the Grell-Devyani scheme for the meteorological cumulus parameterizations, meteorological and chemical tracers would be mixed inconsistently. Now (Li et al., 2019), one can choose the Grell-Freitas cumulus scheme (Grell and Freitas, 2014; Li et al., 2018); used only in RAP-Smoke and RAP-Chem, not HRRR to simultaneously advect meteorological and chemical tracers, as well as represent aerosol wet scavenging. Finally, there is the chemistry connection to microphysics. WRF-Chem v4.6 has two microphysics schemes (Morrison et al. (2005) and Lin et al. (1983)) that are coupled to chemistry such that aerosols are allowed to act as cloud condensation and ice nuclei (CCN and IN). However, these schemes require a chemical

https://doi.org/10.5194/egusphere-2026-4786
Preprint. Discussion started: 13 August 2026

mechanism that distinguishes cloud-borne vs. interstitial aerosols, essentially doubling the number of aerosol tracers, which significantly increases the computational cost of a simulation. The Thompson-Eidhammer microphysics scheme used in RAP/HRRR-Smoke (Thompson and Eidhammer, 2014) takes a more simplified approach, and is "aware" of two aerosol types, water-friendly aerosols (WFA) and ice-friendly aerosols (IFA), which are completely separate from the chemical parameterizations and based on climatology. Though, recent efforts have been made to couple prognostic aerosols with the Thompson-Eidhammer MP scheme, which improved cloud cover predictions of HRRR during the September 2020 North American wildfires (Conrick et al., 2021)

In this work, we further couple the WRF-Chem chemistry packages to the RAP weather forecast model, addressing the aforementioned chemistry-physics coupling inconsistencies. We produce a 24 h forecast for each day of the 1 August – 30 September, 2020 extreme wildfire season in an effort to demonstrate the model improvements as a result of including tighter coupling between chemistry and physics. The manuscript is structured as follows: In Section 2, we describe the RAP-Chem model and code developments, our experimental configurations, and the observational datasets we use to verify our model. Section 3 presents our results, starting with a large-scale overview of model performance and a focus on wildfire-influenced regions. We then highlight the impacts that several chemistry-physics couplings have on forecast skill. Our conclusions are presented in Section 4.

2 Data and Methods

2.1 RAP-Chem

We use an experimental version of the Rapid Refresh (RAP), which is based on the WRF version 3.9 with significant modifications to the physics and dynamics packages (e.g., see (Benjamin et al., 2016). The experimental RAP-Chem forecast (https://rapidrefresh.noaa.gov/RAPchem/) has been running at NOAA GSL since August 2020. The experiments herein use the source code and static fields as of the 17 August 2024 06Z forecast.

RAP-Chem is run with 51 vertical levels from the surface to 10 hPa at a 13.5 km horizontal resolution over a domain that includes North and Central America, as well as parts of South America, Europe, and Asia (Fig. S1a). The lowest model layer is ~8m thick, with the first ~8 layers in the lowest 1 km of the atmosphere; Fig. S1b shows the eta levels provided to the WRF Preprocessing System (WPS). RAP-Smoke uses a meteorological and chemical timestep of 60 s, however here we use 72 s to reduce computation (within the WRF recommended timestep = 6*Δx); no model instability issues occurred using this reduced timestep. Initial and time-varying boundary conditions are provided by the Global Forecast System v16 (GFS, https://www.nco.ncep.noaa.gov/pmb/products/gfs/). Chemical boundary conditions come from the RAQMS forecast model from the University of Wisconsin (Bruckner et al., 2024). An important consideration is that the operational RAP-Smoke undergoes extensive meteorological data assimilation (Benjamin et al., 2016) and the real-time RAP-Chem utilizes the

https://doi.org/10.5194/egusphere-2026-4786
Preprint. Discussion started: 13 August 2026

assimilated input and boundary conditions. Here, however, we do not perform any data assimilation and so meteorological performance is almost surely degraded from that of a simulation with full data assimilation. The model physics options include the Thompson-Eidhammer microphysics scheme (Thompson and Eidhammer, 2014), the Grell-Freitas cumulus scheme (GF; Freitas et al., 2021) with convective removal and parameterized aqueous chemistry turned off. We use the Mellor–Yamada–Nakanishi–Niino eddy-diffusivity mass-flux (MYNN-EDMF) boundary layer (Olson et al. 2026) and surface layer scheme (Olson et al. 2021) with modifications (see Sect. 2.1.1) and the Rapid Update Cycle (RUC) land model (Smirnova et al., 2016). For radiation, we use the Rapid Radiative Transfer Model for GCMS (RRMTG; (Clough et al., 2005)) for both shortwave and longwave radiation schemes and improve physics coupling by supplying RRTMG with prognostic O_3 profiles. For photolysis we use the updated TUV scheme (Madronich and Flocke, 1997) with several modifications. We supply the TUV with GFS total O_3 columns to improve photolysis rate calculations. We also supply TUV with the subgrid clouds simulated by the MYNN-EDMF (see Sect. 2.1.1 and Sect. 3.4.2). Also included in the model is wet removal from resolved precipitation (offline, see below), updated convective wet scavenging (Li et al., 2019, 2018), dry deposition, and gravitational settling.

For gas-phase chemistry, we use a reduced carbon-bond mechanism based on Houweling et al. (1998) with several modifications. The choice of the mechanism's starting point and subsequent modifications were generally performed with the goal of reducing the computational burden of the mechanism while increasing complexity. First, we do not include the transport of radical species or simulate the elemental odd-oxygen species $O^3(P)$ or $O^1(D)$, instead parameterizing them within the photolysis of NO_2 and O_3 like in the Carbon Bond Mechanism v4 (Gery et al., 1989). We also do not simulate methane, instead parameterizing the terminal oxidation products using a globally uniform concentration of 1.8 ppm. A similar approach is used for H_2 with a fixed concentration of 531 ppb. We also added monoterpenes, sesquiterpenes, 2-methyl-3-buten-2-ol (MBO), and IVOC (an intermediate volatility VOC) and their oxidation reactions with OH, O_3, and NO_3 to improve the secondary organic aerosols (SOA) simulations. We additionally updated reaction rates and included the necessary oxidation of organic condensable vapors to simulate SOA. We also include heterogeneous loss of N_2O_5 using a modified parameterizations from the T1_MOZCART chemical mechanism (Schwantes et al., 2020). For SOA, we use a simplified version of the MADE VBS-SOA mechanism described in Ahmadov et al. (2012) similar to WRF-Chem's *chem_opt* = 108. We have also extended our mechanism using *chem_opt* = 109 as a template for including cloud-borne aerosols species to explicitly simulate the indirect aerosol effect, though the results are beyond the scope of this paper. The gas-phase mechanism contains 97 reactions among 48 species, of which 41 are transported. The aerosol mechanism consists of 42 species, three of which are the number concentrations of the three aerosol modes (Aitken, accumulation, and coarse). The real-time RAP-Chem includes two additional aerosol species representing coarse and fine pollen, whose emissions are based on the Pollen Emission for Climate Models (PECM; (Wozniak and Steiner, 2017)); the emissions of these species are not included in the experiments herein, and will instead be described in a follow-up manuscript. Together, the complete chemical mechanism (gases, primary and secondary aerosols) consists of only 90 species, significantly fewer than

https://doi.org/10.5194/egusphere-2026-4786
Preprint. Discussion started: 13 August 2026

operational air quality models (e.g., the US AQM/NAQFC during our simulation period simulated 155 species (https://www.emc.ncep.noaa.gov/mmb/aq/AQChangelog.html)).

Anthropogenic emissions are designed to reflect July 2020, COVID-19 conditions, those used in the real-time forecasts for the 2020 period as described in (He et al., 2023). Over CONUS, the onroad and nonroad portion of our emission datasets are based on the methodology of the gridded Fuel-Based Inventory of Vehicle Emissions (FIVE; see (McDonald et al., 2018)), which is extremely well-suited to capture rapid adjustments to the transportation sector as occurred during COVID-19. Reductions in fuel sales also led to decreases in oil and gas refining as well as refueling emissions (i.e., fugitive VOCs) and so use another fuel use based emission inventory (FOG; (Francoeur et al., 2021)) for oil and gas NOx and VOC emissions. Increased emissions from volatile chemical products (VCPs), key components of urban ozone and SOA formation, was also likely from more frequent and widespread cleaning and disinfecting (McDonald et al., 2018). Area VCP emissions (dominant sector) are modified based on the VCP emission inventory for 2018 (see (Coggon et al., 2021; Stockwell et al., 2021)). Other anthropogenic sectors (e.g., power generation, agriculture) were largely unaffected by the COVID-19 disruptions. In any case, where possible for point sources, we use the Continuous Emission Monitoring System (CEMS) and rely on the NEI-2017 v1 baseline for those sources not reported by CEMS. Outside of CONUS we use the CEDS-2017 inventory (McDuffie et al., 2020). The emissions have a diurnal profile and are delineated by weekday, Saturday, or Sunday. Daily wildfire emissions are generated using the fire radiative power (FRP) method of the RAP/HRRR-Smoke (Ahmadov et al., 2017; Chow et al., 2022; Dowell et al., 2022) and expanded to include emissions of gases and aerosols relevant to our chemical mechanism using (Andreae, 2019). Sea salt emissions are calculated online based on the routines developed for the MADE aerosol module in WRF-Chem. Dust emissions are calculated online with the FENGSHA dust scheme (Campbell et al., 2022).

2.1.1 Improvements to PBL mixing of chemical tracers

As described in the introduction, the default WRF-Chem is configured to perform vertical mixing of chemical tracers alongside dry deposition in the chemical driver using exchange coefficients passed from the PBL driver. Only local mixing occurs, even if using a non-local PBL scheme. Here we update the MYNN-EDMF PBL scheme to enable it to mix chemical tracers alongside the meteorological transported scalars (Olson et al., 2026). The effect of this update is to, by default, perform non-local vertical mixing inside the MYNN-EDMF PBL driver as opposed to dry_dep_driver when using the MYNN-EDMF PBL scheme. During shallow, typically nighttime, boundary layers, surface emissions in a chemical transport model can be unrealistically trapped near the surface due to misrepresentations of mechanical turbulence, which can lead to artificially elevated levels of primary pollutants or artificially low O_3 due to excessive NO_x titration [Huszar et al., 2018a,b; 2020; and references therein]. WRF-Chem attempts to remedy this by modifying the exchange coefficients received from the PBL driver over large emissions sources to simulate unresolved mixing (e.g., traffic turbulence, heat flux from urban areas and fires). The updated exchange coefficient is not passed back to the meteorological model. The modification in the

https://doi.org/10.5194/egusphere-2026-4786
Preprint. Discussion started: 13 August 2026

unmodified WRF-Chem sets a minimum exchange coefficient in the first 11 model layers to 1.0 m^2 s^{-1} if there is any CO emitted by anthropogenic sources. This minimum increases to 2.0 m^2 s^{-1} throughout one-half the model's vertical levels if there are any wildfire CO emissions or when the anthropogenic emissions of CO (or unspeciated $PM_{2.5}$) are greater than 200 mol km^{-2} h^{-1} (0.168 µg m^{-2} s^{-1}). We also include an artificial enhancement in the updated MYNN-EDMF, however, here we do so as a function of emissions of nitrogen oxide (NO) and/or FRP, and only when the PBL height is less than 100 m. Equations (S1–S3) describe the formulation of the enhancements, where *khdz(k)* is the MYNN-EDMF PBL scheme exchange coefficient at model layer *k* normalized by the height (*dz)* and density (*rho*) of the layer, *emis_ant_no* are the anthropogenic emissions of NO and *no_threshold* is set to 10 mol km^{-2} h^{-1} Finally, as described above, we also couple the MYNN-EDMF-simulated subgrid water and ice clouds to the TUV photolysis scheme following the same logic as the already implemented subgrid Grell-Freitas cumulus scheme clouds (also included here).

2.1.2 Aerosol feedbacks

RAP-Chem utilizes the WRF-Chem optical driver with volume averaging in the Mie (Fast et al., 2006) calculations (*aer_op_opt* = 1) to calculate aerosol extinction over four predefined wavelengths. Aerosols are removed via wet scavenging from resolved (*wetscav_onoff* = -1) and convective (*conv_tr_wetscav* = 1) precipitation. The resolved removal is considered to be an "offline" approach since the routine is called from the chemistry driver as opposed to the microphysics; the convective removal is, however, another example of tight chemistry-physics coupling since it occurs inside the Grell-Freitas cumulus scheme (Li et al., 2019, 2018). We have also included a simplified indirect effect in all of the RAP-Chem experiments by coupling the prognostic aerosols to the water-friendly and ice-friendly aerosols (WFA and IFA, respectively) simulated by the Thompson-Eidhammer microphysics scheme. Equations 1-2 in H. Li et al. (2024) describe the conversion of prognostic aerosol mass mixing ratio (µg kg^{-1}) to number concentrations (kg^{1-}). In RAP-Chem, IFA is fine mode dust and WFA consists of the aitken mode fractions of ammonium (NH_4), sulfate (SO_4), POA, SOA as well as sodium and chloride (i.e., sea salt). Simulating the indirect effect in WRF-Chem typically requires a doubling of the number of aerosols (i.e., interstitial and cloud-borne equivalents) whereas in this approach, we utilize tracers already included in the model, thus having only a negligible impact on forecast wallclock time. Evaluating the sensitivity of this parameterization is beyond this work, however, it is another important chemistry-physics connection included in our model.

2.2 Experiments

We perform six simulations of varying length and complexity in an effort to demonstrate the model's fidelity at producing accurate air quality forecasts and to quantify and demonstrate the improvements in the model due to improved physics-chemistry coupling (Table 1).

https://doi.org/10.5194/egusphere-2026-4786
Preprint. Discussion started: 13 August 2026

Table 1. RAP-Chem experiments and configurable options.

Experiment Name	Chemistry Mixing	Enhanced Mixing	Wildfire Plumerise	Direct Feedback	PBL-Photolysis Feedback	Simulation Period (2020)
control	MYNN-EDMF	yes	yes	yes	yes	1 Aug – 30 Sep
no_dirfdb	MYNN-EDMF	yes	yes	no	yes	1 Aug – 30 Sep
newmix	MYNN-EDMF	no	no	no	yes	1-7 Aug
oldmix	WRF-Chem	no	no	no	yes	1-7 Aug
enhmix	MYNN-EDMF	yes	no	no	yes	1-7 Aug
phtmix	MYNN-EDMF	yes	no	no	no	1-7 Aug

Our primary experiment (*control*) covers a two month period (1 August – 30 September, 2020) during which the US experienced sustained poor air quality due to massive wildfires burning in the West (e.g., Zhou et al, 2021, Higuera et al., 2021). Figure S2 shows the integrated FRP over the time period highlighting two distinct burning periods, though the integrated FRP during September was more than double that in August. The *control* experiment includes all of the improved physics-chemistry coupling described above, and we consider it to be our reference experiment. The experiment *no_dirfdb* turns off the direct aerosol effect (*aer_ra_feedback* = 0), and is also simulated over the full two-month period. Four simulations are used to quantify changes due to the updates to MYNN-EDMF (Sect. 2.1.1). The *oldmix* simulation performs mixing following the default mixing method of WRF-Chem v3.9 (Powers et al., 2017; Skamarock et al., 2008) with one modification to the source code: In the original WRF-Chem subroutine *dry_dep_driver*, the exchange coefficients obtained from the PBL scheme are artificially enhanced in half of the vertical levels for grid cells with fire emissions or large anthropogenic emissions (so long as urban physics is not in use (i.e., *sf_urban_physics* = 0) and CO is an emitted species). For *oldmix*, we turn off this default enhanced mixing. The experiment *newmix* utilizes the updated mixing code, also not including the enhancement routines described above. An additional sensitivity experiment (*enhmix*) is conducted to demonstrate the utility of enhanced mixing inside the MYNN-EDMF scheme over urban and wildfire grid cells. In a final experiment, (*phtmix*), we do not include the effect of subgrid clouds simulated by MYNN-EDMF in the photolysis scheme. In all **mix* experiments, we do not invoke the wildfire plume rise parameterization such that no other routines impact the vertical redistribution of emissions and a fair comparison between the old and new mixing routines can be made. Moreover, we also do not simulate aerosol feedback to meteorology (i.e., like *no_dirfdb*). As such, we focus on the 1-7 August 2020 time period for the **mix* experiments to avoid simulating a period with an excessive number of fires in the domain (see Fig. S2). We initialize the forecasts at 00Z each day with GFSv16 meteorological fields; chemical fields are cycled between successive simulations (i.e., no chemistry initializations beyond the first day initialized with RAQMS). We consider the first 3 days (29-31 July, 2020) of *control* a spin-up period and discard from the analysis. The *no_dirfdb,* and **mix* experiments are initialized on 1 August 2020 and branch from *control*. All of our experiments cover the entire RAP domain, though we frequently display results over CONUS or one of the 10 US EPA regions (EPA, 2025).

https://doi.org/10.5194/egusphere-2026-4786
Preprint. Discussion started: 13 August 2026

2.3 Observations

To evaluate the RAP-Chem experiments, we use a variety of surface and remotely-sensed observational datasets. For meteorological evaluation, we use the NOAA Integrated Surface Database (ISD, also referred to as ISH/ISH-lite; https://www.ncei.noaa.gov/products/land-based-station/integrated-surface-database), using observations of 2-m temperature (T_{2m}), 2-m dew point temperature (Td_{2m}), 10-m wind speed (U_{10m}), visibility (VIS), and precipitation. We also utilize measurements of total, direct, and diffuse downwelling shortwave radiation from seven SURFRAD and five SOLRAD sites across CONUS (Augustine et al., 2005, 2000) operated by NOAA Global Monitoring Laboratory (GML). For air composition, we primarily use the USA EPA AirNOW network (https://www.airnow.gov/about-the-data/), which includes stations in the US, Canada, and Mexico. This data is provided in near real-time and is best suited for real-time evaluation of forecast models. Composition variables considered include surface O_3, $PM_{2.5}$, nitrogen dioxide (NO_2), and carbon monoxide (CO). We also utilize NASA's AErosol RObotic NETwork (AERONET; Holben et al., 1998, 2001) stations to perform verification of aerosol optical depth at 550 nm (AOD_{550}). We also utilize NASA's AQUA AIRS retrievals of CO vertical profiles (https://airs.jpl.nasa.gov/mission/overview/).

3 Results

3.1 Meteorological performance

We evaluate the meteorological performance of *control* against surface measurements from the NOAA ISD using the newly developed MELODIES MONET, a modular framework that integrates diverse atmospheric chemistry observational datasets with chemistry model results for the evaluation of air quality and atmospheric composition (https://melodies-monet.readthedocs.io/en/stable/). Fig. S3 shows the spatial bias plots for T_{2m}, Td_{2m}, U_{10m}, VIS, and the time series of total daily precipitation over the RAP-Chem domain. In general, the model performs very well for each of the meteorological parameters, which is somewhat expected given that the foundation of the RAP-Chem is the operational numerical weather prediction (NWP) forecast system, RAP-Smoke (though here we do not include the data assimilation or hourly cycling that is performed in RAP-Smoke). T_{2m} is generally biased low (about -1°C) in much of Canada, Mexico, and the eastern US, while biased high (~1–3°C) over the western regions heavily impacted by smoke, initially indicating a low bias in simulated aerosols and/or their radiative extinction. Averaged over CONUS, the mean bias (MB) is very small (-0.1°C). Td_{2m} is generally well simulated (CONUS MB = -0.4°C) except for the smoke influenced regions where it is biased low by 2–5°C. Wind Speed is generally biased high (~0–2 m s^{-1}) though there are some small negative biases in the US West. Visibility diagnostics are often utilized by those in aviation, and accurate forecasts are critical to maintaining smooth flight operations. RAP-Chem uses the same visibility diagnostics as the operational RAP/HRRR-Smoke system, though in RAP-Chem, aerosols beyond smoke are accounted for in the extinction calculation. Outside of the central US where RAP-Chem is biased low in visibility (0–2 km), visibility is generally overpredicted, up to 5 km greater than observations in

https://doi.org/10.5194/egusphere-2026-4786
Preprint. Discussion started: 13 August 2026

the most heavily smoke-influenced regions (CONUS MB = 2067 m). Paired with the temperature biases, these biases indicate large underestimations in near surface smoke concentrations. Precipitation is biased slightly high averaged over CONUS (~0.1 mm), though much larger underestimations (>2 mm) are found in the central United States through the path of Hurricane Laura where daily rainfall totals exceeded 25 mm (not shown).

3.2 Surface air quality and AOD performance

Figure 1a-b shows the 1 August – 30 September, 2020 time series of RAP-Chem simulated maximum daily 8-h average (MDA8) surface O_3 and 24-h averaged $PM_{2.5}$ compared with EPA AirNOW monitors in the CONUS. Figures S4-S5 show the same time series over each of the 10 EPA regions as well as the average observed values over the time period for each station overlain on the average field of each model simulation. The normalized mean bias (NMB) for each simulation compared to each EPA region over each of the experiment's respective simulation periods is in Table 2.

Table 2. Normalized Mean Bias (NMB, %) for MDA8 O_3 (ppb) and 24-h average $PM_{2.5}$ (μg m^{-3}) over 1 August - 30 September, 2020 for *control* and *no_dirfdb* and 1-7 August, 2020 for **mix*.

O_3	***US***	***R1***	***R2***	***R3***	***R4***	***R5***	***R6***	***R7***	***R8***	***R9***	***R10***
control	6.6	13.3	10.8	6.1	14.1	-1.5	1.7	-0.7	-1.1	11.2	22.4
no_dirfdb	9.5	15.2	13.3	8.2	14.7	1.4	-3.5	2.3	2.2	15.9	33.7
oldmix	4.3	14.1	10.3	1.9	2.5	1.7	-4.8	-6.4	-3.0	17.5	14.5
newmix	4.6	13.7	8.6	2.1	2.3	3.7	-13.6	-4.7	-2.2	17.5	16.0
enhmix	4.6	13.7	8.5	2.1	2.3	3.8	-4.8	-4.5	-2.2	17.4	16.0
phtmix	8.2	15.8	12.8	8.1	9.7	10.0	-1.4	-1.5	-2.0	16.3	16.3
PM2.5	***US***	***R1***	***R2***	***R3***	***R4***	***R5***	***R6***	***R7***	***R8***	***R9***	***R10***
control	-15.8	3.0	89.5	53.9	39.6	25.6	22.6	33.9	-17.5	-34.0	-44.1
no_dirfdb	-16.8	3.7	88.1	53.7	39.4	25.8	23.3	34.3	-13.6	-34.0	-48.7
oldmix	10.9	-17.9	67.8	54.6	4.2	27.2	21.2	45.3	-10.6	2.5	-15.9
newmix	9.6	-17.9	66.9	49.0	0.3	26.9	18.8	46.9	-11.4	1.0	-16.3
enhmix	7.2	-19.1	54.2	47.0	-1.8	23.6	16.7	39.6	-13.3	0.0	-17.0
phtmix	10.9	-17.4	64.9	55.3	4.0	28.1	20.4	42.2	-12.5	-0.2	-16.7

https://doi.org/10.5194/egusphere-2026-4786
Preprint. Discussion started: 13 August 2026

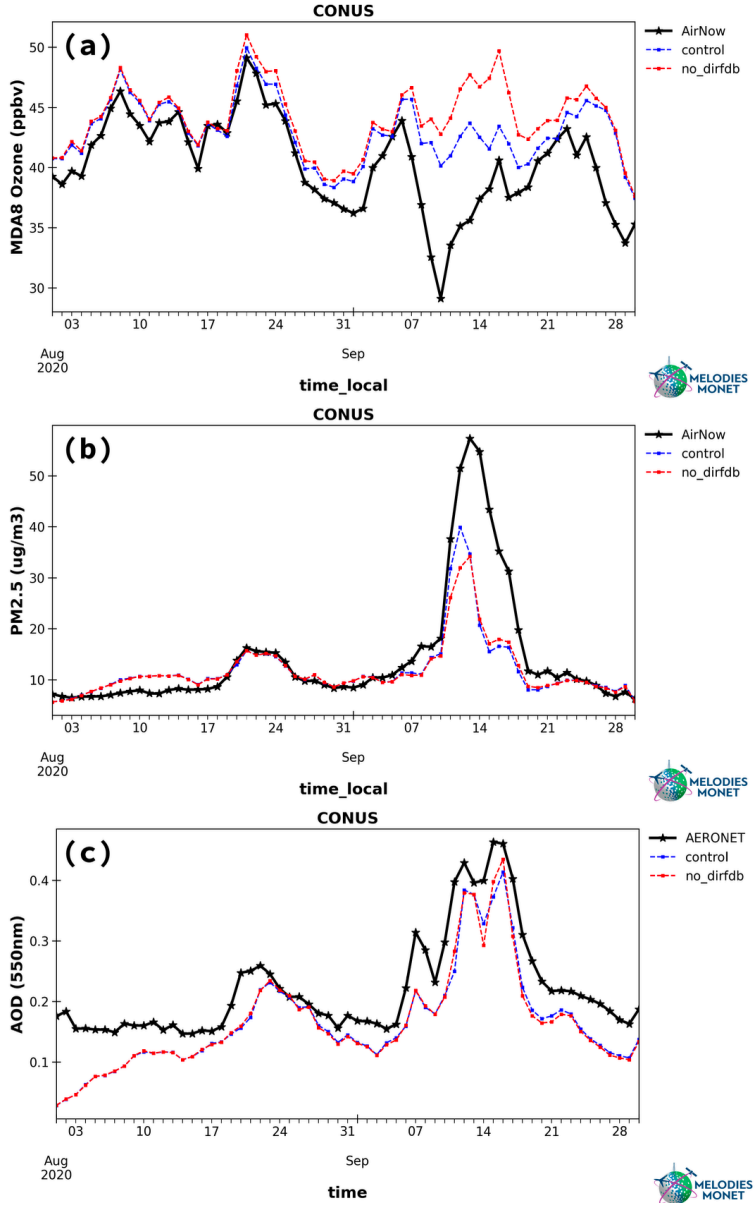

Figure 1. Time series (1 August – 30 September, 2020) of (**a**) MDA8 O_3, (**b**) daily average $PM_{2.5}$ observed by EPA AirNOW and (**c**) daily average AOD_{550} as observed by AERONET compared to those simulated by the *control* and *no_dirfdb* experiments. EPA AirNow data courtesy of the U.S. Environmental Protection Agency. AERONET data courtesy of NASA.

For O_3, RAP-Chem *control* performs well over CONUS until a period of observed sharp decreases in O_3 during the first half of September. This period is better captured by *control* compared to *no_dirfdb* and is explored in Sect 3.3 and 3.5. RAP-Chem *control* matches the observational variability with minimal normalized mean bias (NMB) and RMSE in all EPA regions (NMB = -1.5% to 22.4%; RMSE = 6.3 to 15.2 ppb). Air quality models frequently demonstrate high O_3 biases in

https://doi.org/10.5194/egusphere-2026-4786
Preprint. Discussion started: 13 August 2026

EPA Region 4 (US Southeast), often attributed to large and variable sources of biogenic (e.g., (Guo et al., 2018) and agricultural burning emissions (Tang et al., 2022). In EPA Region 4, RAP-Chem *control* does a remarkable job during the first half of the month of August, but exhibits a ~2-3 ppb systematic bias during the second half of August and then again during the beginning and end of September (Fig. S4). It's unclear why the model performs poorly here, but it may be related to precipitation events not properly scavenging precursor species. In EPA Region 5 (upper Midwest), RAP-Chem *control* performs exceptionally well in August, with the only notable deficiency being slightly underestimated minima. It generally captures the daytime peaks during the first half of the month, but is biased low by ~5 ppb during the latter half. The average diurnal profile of O_3 averaged over CONUS and each of the EPA regions (Fig. S6) reveals biases are often positive during the day (8AM–8PM) and negative at night (8PM–8AM), resulting in a more pronounced diurnal cycle as compared to the observations. Overall, the shape of the diurnal cycle of O_3 is captured well.

RAP-Chem simulates $PM_{2.5}$ with less skill than O_3, largely due to the extreme influence from the wildfires during the experimental period, but also partially due to overestimated emissions in urban areas. (i.e., many EPA AirNOW monitors are located in urban locations with significant traffic influence and therefore can overstate the influence of those regions). Indeed, the emissions of unspeciated $PM_{2.5}$ were logarithmically transformed to limit this bias. In all non-wildfire source regions (R1-R7), RAP-Chem tends to largely overestimate both the variability and magnitude of $PM_{2.5}$. It is likely that the diurnal cycle of urban (e.g., traffic) emissions needs further modification given the location of the biases (cities) and the species responsible.

Figure 1c compares observed and modeled AOD_{550} at 20 AERONET sites within the RAP-Chem domain for the simulation period. Overall, RAP-Chem *control* is biased low in AOD_{550} at most locations and CONUS (NMB = -17.5%), resulting from a combination of low bias in simulated $PM_{2.5}$ (Fig 1b), incorrect vertical distributions of aerosols, and/or inaccurate representations of the aerosols' refractive indices. Indeed, if AOD_{550} is instead calculated with a look-up-table (LUT) approach based on the EPA IMPROVE algorithm (Malm et al., 1994) AOD_{550} improves at some sites (e.g., Fig. S7) during peak extinction periods, but the LUT approach tends to significantly overestimate background AOD_{550}. While a physically-based approach to calculating aerosol extinction is often desired, some forecast systems may prefer a LUT approach that can be easily tuned and requires minimal computational requirements over the more expensive Mie-calculated extinction used here and associated uncertainties in mixing state assumptions (e.g., volume averaging vs. internally mixed).

3.3 Wildfire region performance

The August-September 2020 period was one of the most active and destructive wildfire seasons in the Western US to date. EPA Regions 8, 9, and 10 were significantly inundated by heavy smoke as well as an influx of O_3 precursors species (i.e., NO_x and VOCs) leading to sustained poor air quality in all three regions (e.g., Fig S4-5, (Higuera and Abatzoglou, 2021; Zhou et al., 2021).

https://doi.org/10.5194/egusphere-2026-4786
Preprint. Discussion started: 13 August 2026

For EPA region R8, RAP-Chem shows generally good agreement overall for both O_3 and $PM_{2.5}$ during both months. In August, both *control* and *no_dirfdb* underestimate peak $PM_{2.5}$ abundances (e.g., August 19-20, 24-26), but they are much better simulated by *control*. For O_3, both RAP-Chem simulations are biased low through August and biased slightly high in September, though *control* has significantly smaller biases compared to *no_dirfdb*, nearly 10 ppb on some days. In September, both simulations again produced excellent $PM_{2.5}$ predictions in R8 outside of the false alarm on September 14th seen in both experiments (though to a lesser extent in *control*). For O_3, both *control* and *no_dirfdb* struggle to capture nighttime lows.

In EPA region R9, RAP-Chem shows relatively good agreement overall for both O_3 and $PM_{2.5}$, but less so compared to R8. As in R8, RAP-Chem struggles to capture the nighttime O_3 low during both months, likely resulting from too little titration in the nocturnal PBL. The nighttime bias also likely contributes to the systematic ~10 ppb bias in the day during the end of August and middle of September. Peak O_3 is generally overestimated in RAP-Chem in EPA R9. Some improvements are seen in the *control* compared to *no_dirfdb*, though the impact is relatively small. For $PM_{2.5}$, RAP-Chem mostly captures the peak abundances in August in both experiments, but both simulations fail to capture the mid-month peak in September.

In EPA region R10, surface O_3 is mostly simulated extremely well, especially by *control*, which accurately captures large decreases in O_3 from 9-14 September due to reductions in temperature and photolysis rates from overhead smoke. RAP-Chem *no_dirfdb* overestimates O_3 by almost 70 ppb demonstrating the importance of capturing aerosol impacts on radiation and photolysis. During September, RAP-Chem *control* captures the $PM_{2.5}$ increases through around 12 September, but then misses the buildup that continues to occur through 15 September. However, RAP-Chem *control* simulates ~50 µg m^{-3} more than *no_dirfdb*, dramatically improving predictions for several days.

Figure S8 shows the correlation between the bias in hourly O_3 with the bias in hourly $PM_{2.5}$ for both *control* and *no_dirfdb*, illustrating the complex interplay between urban chemistry, wildfire smoke – both near the source and transported, and the impact of the aerosol feedback on radiation.

In *no_dirfdb,* strong negative correlations are seen along the northern half of the west coast, and positive correlations in regions directly downwind of the wildfire locations in the upper Intermountain West. The strong negative correlations along the West Coast are due to the model over predicting the amount of surface insolation and thus the photochemistry of combined anthropogenic and wildfire emissions. This is despite the low biases in $PM_{2.5}$ because there was still large amounts of smoke and precursors that reached these areas. In *control*, this correlation is significantly reduced because the model simulated much less ozone with roughly the same amount of precursor. Downwind of the wildfires (e.g., Montana),, the correlations are positive, and much stronger in *no_dirfdb.* When *no_dirfdb* underpredicts the smoke and precursor input it

https://doi.org/10.5194/egusphere-2026-4786
Preprint. Discussion started: 13 August 2026

also leads to an underprediction of ozone. Conversely, because the models generally overpredict the amount of smoke downwind (e.g., Fig. S4),, the correlations in *no_dirfdb* are large and positive because there is no reduction in solar insolation. In *control*, these correlations are much smaller due to the aerosol feedback reducing the amount of active photochemistry.

3.4 Improved chemistry-physics coupling in the PBL scheme

3.4.1 Vertical mixing

Here we compare the **mix* simulations to quantify the improvements of the chemistry coupling to MYNN-EDMF. Figure 2a-c displays domain-wide average surface differences (*newmix* minus *oldmix*) of key chemical species (O_3, CO, and $PM_{2.5}$) over the 1-7 August 2020 test period. Overall, all four *_*mix* simulations are similar to *control* in that they show good O_3 prediction skill and in general are biased low compared to observations (Table 2), though *control* remains the best simulation. Small but systematic differences in O_3 are found between *oldmix* and *newmix* (±2 ppb). Much larger changes are seen when incorporating the enhanced mixing (*enhmix* minus *newmix*, Fig 2d-f). Enhanced mixing generally has the effect of increasing surface O_3 at night, as the added enhancement reduces NO titration and can bring elevated O_3 from the residual layer to the surface (Hu et al., 2012). Enhancement also increases the surface O_3 daily maximum, likely due to increased O_3 and precursor availability from the previous night since the enhancement switch is only very rarely activated during the daytime due to the condition for low PBL heights. For $PM_{2.5}$, differences between *newmix* and *oldmix* are very minimal when averaged over the EPA regions, though *enhmix* consistently predicts lower $PM_{2.5}$ concentrations during the daily peak, improving the model performance in 7 of 10 EPA Regions (Table 3). Over urban areas and directly over wildfires, *newmix* has higher $PM_{2.5}$ concentrations. Downwind of the large fire in California, however, *newmix* shows large reductions indicating more smoke is lofted above the surface compared to *oldmix* (recall plume rise parameterizations are disabled in all **mix* simulations). Compared to *newmix*, *enhmix* simulates a relatively uniform increase of $PM_{2.5}$ (~1-3 ug m^{-3}), of which most of the difference occurs in the first three days of the simulations. Similar to $PM_{2.5}$, *newmix* CO is in general lower compared to *oldmix* but elevated over urban locations and wildfires. Additionally like $PM_{2.5}$, lower concentrations are also observed downwind of wildfires. Compared to *newmix*, *enhmix* simulates lower CO concentrations over urban areas, however increases are seen over most of the domain.

https://doi.org/10.5194/egusphere-2026-4786
Preprint. Discussion started: 13 August 2026

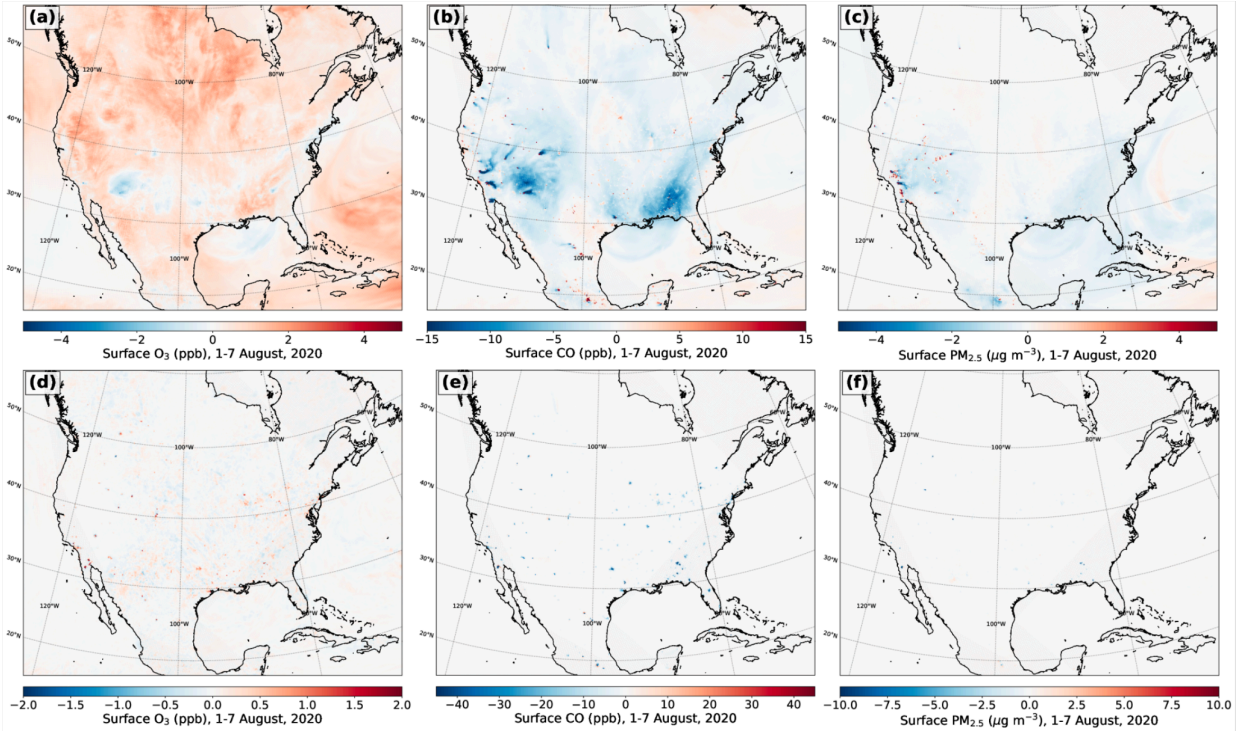

Figure 2. Average surface differences for (**a-c**) *newmix* minus *oldmix* for surface (**a**) O_3, (**b**) CO, and (**c**) $PM_{2.5}$ and (**d-f**) *enhmix* minus *newmix* for surface (**d**) O_3, (**e**) CO, and (**f**) $PM_{2.5}$

The nonlocal mixing component of the MYNN-EDMF allows mass and momentum exchanges between non-adjacent model layers, which is particularly important during periods with deep boundary layers. Figure 3 provides an example of the changes in CO abundances as a result of the MYNN-EDMF changes over a grid cell near Phoenix, AZ. Compared to an EPA AirNOW surface measurement (Fig. 3a), each of the simulations reproduce the CO time series modestly well, particularly during the first four days. During the final three days, the model tends to overestimate the daily midday peaks, potentially related to overestimated urban emissions. Only very small differences in CO are seen between the simulations, with the largest differences seen in the simulations that include the modified enhancement equation. Fig 3b-d shows the CO time series over the same grid cell as a function of height for the *oldmix*, *newmix*, and *enhmix* simulations overlain by CO observations from AQUA AIRS. These plots reveal enhanced CO throughout the PBL for all three simulations, and in general underestimate compared to AQUA AIRS. Comparing the differences (Fig. 3e and 3f) reveals a consistent pattern of *newmix* simulating increased CO at the surface (~5 ppb) and towards the top of the PBL (up to 25 ppb) and reduced CO in between (around -20 ppb). Another interesting feature is elevated CO in *newmix* throughout the column as the PBL grows, particularly in the final days of the simulation period.

https://doi.org/10.5194/egusphere-2026-4786
Preprint. Discussion started: 13 August 2026

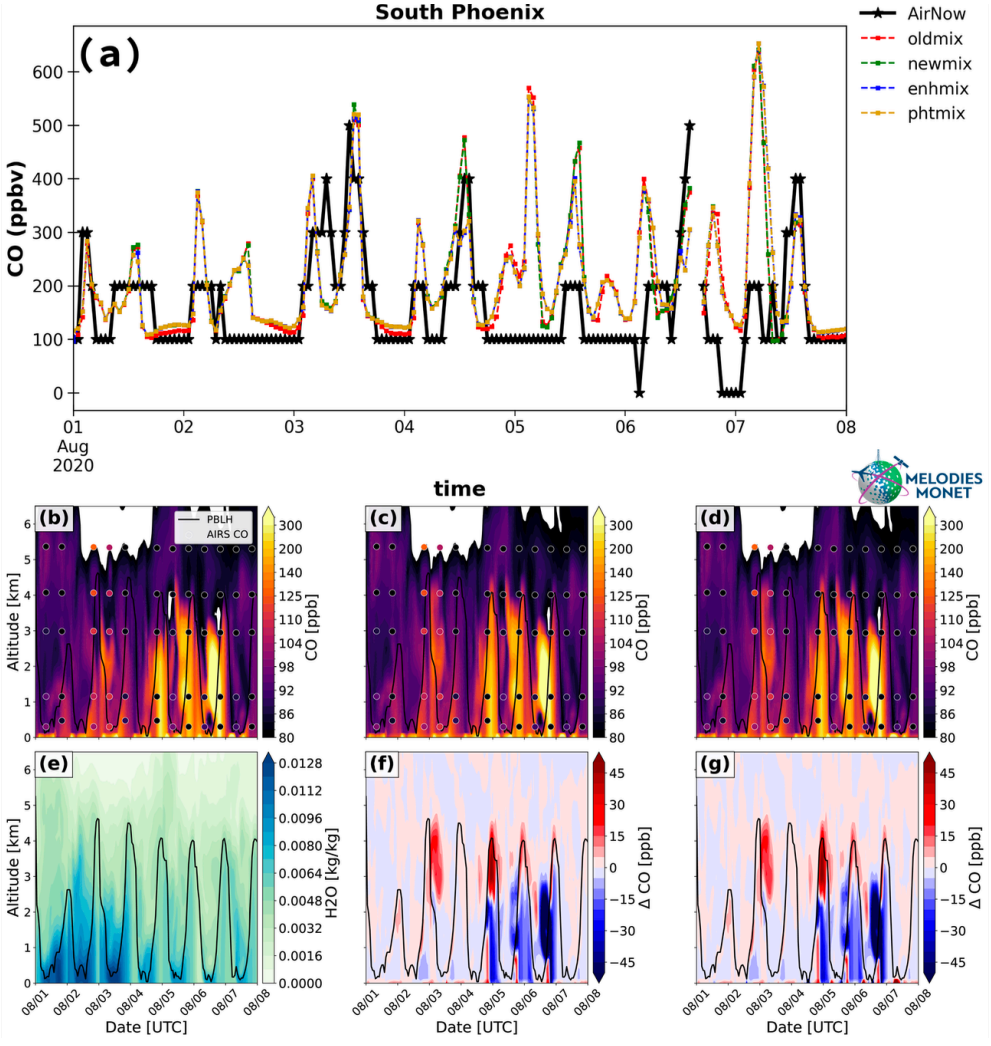

Figure 3. (**a**) Time series of surface CO for each of the **mix* experiments and compared to observations from AirNOW monitoring site South Phoenix. **(b-d)** Time series of the vertical profile of CO mixing ratio in (**b**) *oldmix* (**c**) *newmix* and (**d**) *enhmix*. Colored circles show observations by the AIRS instrument aboard the AQUA satellite. Black lines denote the model-diagnosed PBL height (**e**) Water vapor mixing ratio in *newmix*. (**f**) Difference (*newmix* minus *oldmix*) in CO mixing ratios. (**g**) Difference (*enhmix* minus *oldmix*) in CO mixing ratios. EPA AirNow data courtesy of the U.S. Environmental Protection Agency. AIRS data courtesy of NASA.

Figure 5 provides a similar layout as Figure 4, but here for a shallow convection case near northern Georgia (including the grid cell over the EPA Monitor South Dekalb located at 33.69 N, 84.27 W). Clouds extend from ~1 km/900 mb through ~5 km/600 mb throughout the region and below the clouds (not shown), and *newmix* CO concentrations are lower compared to *oldmix*, while they are higher above the boundary layer clouds. Compared to an EPA AirNOW surface measurement at South DeKalb (Fig. 4a), each of the simulations reproduce the shape of the CO time series modestly well, though tending to underestimate observed CO, especially at night when the observations are at their highest. Only very small differences in CO are seen between the simulations at the surface, again primarily from the simulations that include the modified enhancement

https://doi.org/10.5194/egusphere-2026-4786
Preprint. Discussion started: 13 August 2026

equation. Larger differences are seen aloft. For example, Fig 4b-d shows the CO time series over the same grid cell as a function of height for the *oldmix*, *newmix*, and *enhmix* simulations overlain by PBL height and observations from AQUA AIRS. The difference between *newmix* and *oldmix* reveals a consistent pattern of *newmix* simulating increased CO (~10 ppb) above the PBL, and decreases (10-20 ppb) below it, similar to that found in Phoenix. The decreased CO through ~2km improves the bias since *oldmix* tends to overestimate CO in the lower layers above the surface. For the second half of the simulation, we can see significant increases aloft in the *enhmix* case, though this tends to disagree with the observations. Overall, the correlation with AIRS CO improves in *newmix* and *oldmix* for both the daytime ascending (Fig. S9) and nighttime descending (Fig. S10) modes. The correlations do not improve as substantially in *enhmix* compared to *newmix*, though the largest improvements are seen over urban locations for the nighttime descending mode (i.e., where and when the enhancement would be active).

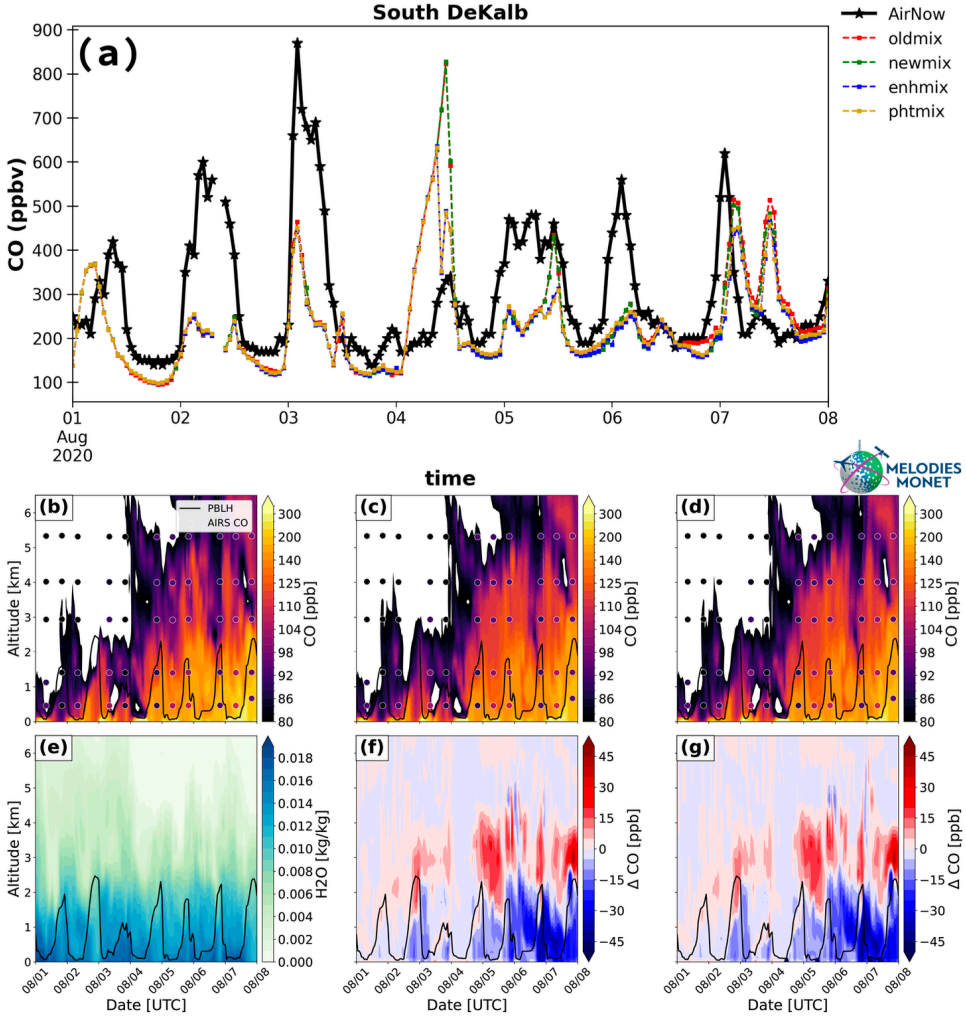

Figure 4. As Fig. 3, but for a location near Atlanta, GA (South Dekalb, 33.69 N, 84.27 W). EPA AirNow data courtesy of the U.S. Environmental Protection Agency. AIRS data courtesy of NASA.

https://doi.org/10.5194/egusphere-2026-4786
Preprint. Discussion started: 13 August 2026

3.4.2 Photolysis coupling to subgrid clouds in MYNN-EDMF

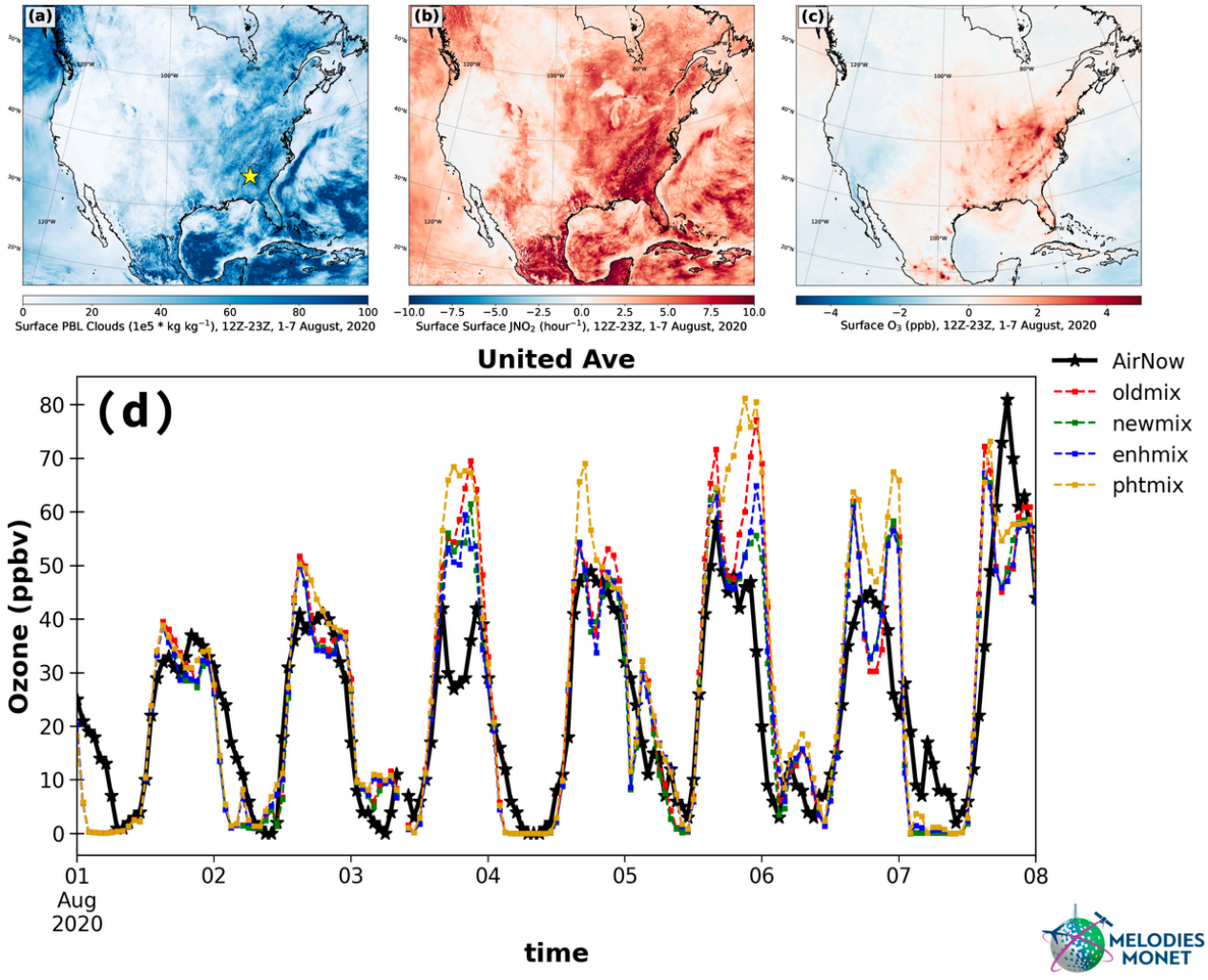

Figure 5. (**a**) Average daytime (12-23Z) total cloud (water + ice) column from MYNN-EDMF in *newmix*, (**b**) average daytime differences (*phtmix* minus *enhmix*) in surface photolysis rates of NO_2 and (**c**) surface O_3 from 1-7 August. (**d**) Time series of *_*mix* simulated and observed surface O_3 at the EPA AirNOW site United Ave over the same period. The location of the United Ave AirNow site is shown in (a). EPA AirNow data courtesy of the U.S. Environmental Protection Agency.

In the WRF-Chem TUV scheme, several options exist to include the impacts of clouds, both those that are resolved in the microphysics scheme and those parameterized in the Grell-Freitas, Grell-Devyani, or G3 cumulus scheme. The *phtmix* experiment removes this impact included in *oldmix*, *newmix*, and *enhmix*, allowing a quantification of the impact of the subgrid boundary layer water and ice clouds simulated by the MYNN-EDMF scheme on photolysis and resulting photochemistry. Figure 5a shows the total column boundary layer cloud concentrations averaged over daytime hours (12Z – 23Z) of the simulation period in *phtmix*. Boundary layer clouds are simulated at a maximum in the Southeast and

https://doi.org/10.5194/egusphere-2026-4786
Preprint. Discussion started: 13 August 2026

Appalachia, with almost no BL clouds simulated in western states. Fig 5b shows the average difference (*phtmix* minus *enhmix*) in surface daytime photolysis rates of NO_2 (jNO_2), which closely follows the pattern of BL clouds. Expectedly, Fig. 5c shows daytime O_3 reductions throughout most of the eastern US ranging from ~1 to 8 ppb. Small increases (~1 ppb) are found throughout the Mojave desert. Here the increased O_3 is likely related to the Apple wildfire in southern California. Finally, Fig. 5d shows the impact at a single site (United Ave, 33.72°N, 84.36°W). During most of the period, only small differences can be seen between the simulations. On August 3, however, the *phtmix* simulation overpredicts daytime ozone to a similar degree as *oldmix*. On August 5, *phtmix* overpredicts daytime O_3 by over 30 ppb, but the other simulations (*oldmix*, *newmix*, and *enhmix*) that include boundary layer cloud impacts on photolysis accurately capture observed O_3.

3.5 Aerosol feedback: direct effect

The RAP-Chem includes the direct aerosol feedback by calculating the extinction of aerosols using Mie theory and providing that extinction to the model's radiation and photolysis schemes. The direct aerosol effect acts to reduce available radiation, which can lead to, among other things, stabilization of the boundary layer and reduction in photolysis rates. A shallower stable boundary layer allows pollutants to accumulate near the surface, however, for some secondary pollutants like O_3, this can lead to decreases in their abundance due to nonlinear chemistry. Reductions in photolysis rates will also contribute to decreases in surface O_3. Overall, averaged over CONUS, surface O_3 is ~1 ppb higher in *no_dirfdb* compared to *control,* with both MB and RMSE improvements (2.4 to 1.4 and 13.2 to 12.2, respectively). The *control* experiment has a lower RMSE compared to *no_dirfdb* in 7 out of 10 EPA regions, most notably in the wildfire regions (see Sect. 3.3). To further demonstrate the improvements in the model due to the direct aerosol effect, we focus on Washington state in EPA Region 10 during September 2020 when aerosol concentrations were extremely high and thus the aerosol feedback is also strong. Figure 6a shows the time series of observed hourly $PM_{2.5}$ compared to the *control* and *no_dirfdb* simulations averaged over all AirNow sites in Washington. Overall, *control* accurately predicts the surface aerosol enhancement from 7-13 September with *no_fdb* simulating $PM_{2.5}$ concentrations that are ~50 ug m-3 lower than *control* (and more biased compared to observations). This forecast deficiency was widely noted in the then-experimental RAP/HRRR-Smoke forecast model as well as other operational models (e.g., the NAQFC) and is still an area of active investigation (e.g., Conrick et al., 2021). Figure 6b shows the T_{2m} time series over the same period. The *control* simulation demonstrates excellent skill at reproducing the observed time series, accurately capturing the decreases in temperature due to high aerosol loadings that *no_dirfdb* misses. This impact is also seen in the surface O_3 time series (Fig 6c) where the aerosol direct effect in *control* reduces surface O_3 over EPA Region 10 by ~40 ppb compared to *no_dirfdb*, allowing *control* to accurately capture the reduced O_3 production seen in the observations.

https://doi.org/10.5194/egusphere-2026-4786
Preprint. Discussion started: 13 August 2026

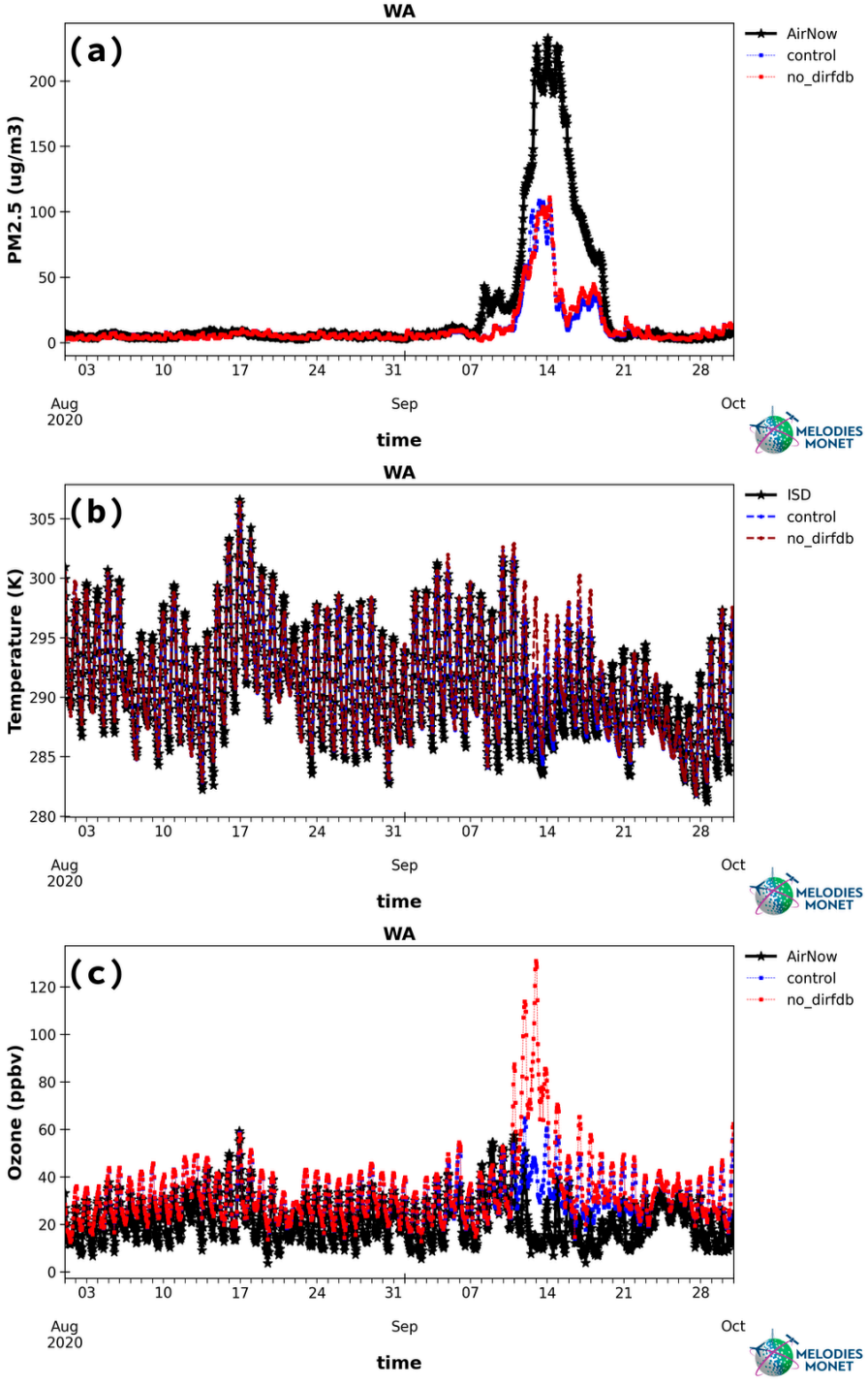

Figure 6. Time series (1 Aug - 30 Sep, 2020) of hourly (a) surface $PM_{2.5}$, (b) 2-m temperature, and (c) surface O_3 averaged over Washington state for *control*, *no_dirfdb*, as compared to EPA AirNOW (a,c) and NOAA ISD (b) monitors. EPA AirNow data courtesy of the U.S. Environmental Protection Agency. NOAA ISD data courtesy of the National Oceanic and Atmospheric Administration.

https://doi.org/10.5194/egusphere-2026-4786
Preprint. Discussion started: 13 August 2026

It is important for the model to not only simulate the total amount of radiation reaching a model layer, but also the type of that radiation (i.e., direct vs. diffuse). Figure 7 shows the diurnal cycle of total, direct, and diffuse radiation averaged over all the SURFRAD and SOLRAD sites as compared to *control*, and *no_dirfdb*. RAP-Chem *control* matches the observations of total irradiance well (MB= 6.0 W m^{-2} averaged across all sites) while *no_dirfdb* is expectedly biased high (18.4 W m^{-2}) . For direct irradiance only, both RAP-Chem experiments are biased high, but including the aerosol effect drastically reduces the bias (from 127.1 to 61.3 W m^{-2}). Conversely, diffuse radiation is increased by including the direct effect, and as such the bias in RAP-Chem *no_dirfdb* for diffuse irradiance is drastically reduced in RAP-Chem *control* (-16.9 vs. 2.3 W m^{-2}). We find the biases in irradiance increase as the overhead aerosol column amount increases (not shown).

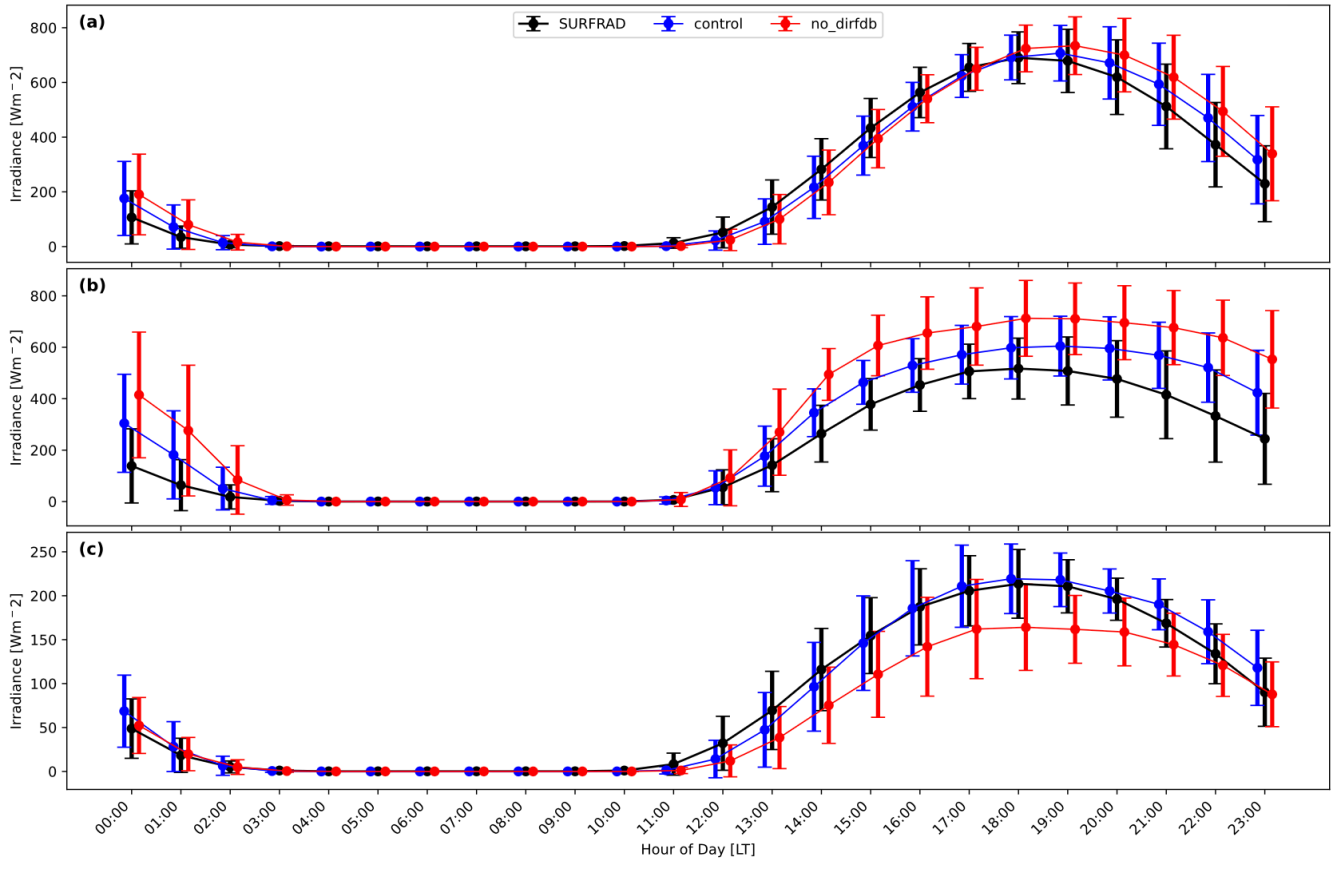

Figure 7. Diurnal cycle (UTC) of (**a**) total, (**b**) direct, and (**c**) diffuse radiation averaged over all available SURFRAD and SOLRAD sites (black) as compared to the *control* (blue) and *no_dirfdb* (red) simulations. SOLRAD and SURFRAD data courtesy of the National Oceanic and Atmospheric Administration.

https://doi.org/10.5194/egusphere-2026-4786
Preprint. Discussion started: 13 August 2026

4 Conclusions

Here we present retrospective experiments with the experimental Rapid Refresh model coupled to Chemistry (RAP-Chem), a coupled meteorology-chemistry model operating in real-time at NOAA GSL since the fall of 2020. Our primary simulation includes our real-time configuration and was performed during a period of intense wildfire activity in North America (1 Aug – 30 Sep, 2020) to evaluate the fidelity of the model to reproduce observed air composition and accompanying meteorology. This primary experiment includes multiple existing and new developments in chemistry-physics coupling, including:

1. Coupling of updated aerosol scheme to the radiation (RRTMG) and photolysis (TUV) schemes
2. Online, convective transport and wet scavenging within the Grell-Freitas cumulus scheme
3. Online, non-local mixing of chemical scalars in the MYNN-EDMF PBL scheme
4. Coupling of the MYNN-EDMF PBL clouds in the TUV photolysis scheme
5. Coupling of prognostic aerosols to WFA and IFA in the Thompson-Eidhammer MP scheme.

Overall, we find that the RAP-Chem, despite using a relatively simple gas-phase mechanism, is able to simulate the salient features of observed surface O_3 and $PM_{2.5}$ as well as demonstrate skill in predicting enhancements (or reductions) of O_3 and $PM_{2.5}$ due to wildfires. A separate experiment *no_dirfdb* evaluates the impact of (1) by turning off the aerosol direct effect. In most cases, including the direct aerosol effect improves model predictions for surface ozone, particulate matter, and the accompanying meteorology. Surface $PM_{2.5}$ is generally underestimated in wildfire source regions as well as the extinction of those aerosols (e.g., underestimated AOD_{550}). However, during periods of peak underestimation, a simpler look-up-table approach captures this extinction, providing insight into potential modifications to the wildfire emission factors and/or the aerosol refractive indices and hygroscopicity used in the Mie calculations.

Further, we have performed four sensitivity simulations (i.e., **mix*) to evaluate the improvements in the model due to the (3) inclusion of online (i.e., coupled, within the physics), non-local mixing inside the MYNN-EDMF PBL scheme, artificially enhancing near-surface exchange coefficients and (4) inclusion of parameterized PBL clouds in the TUV photolysis scheme. In general, the impact of new mixing is best seen in the distribution of CO abundances, where the updated mixing is able to loft and thus increase primary pollutant abundances higher in the atmosphere, thereby reducing abundances closer to the surface. Average ozone at the surface, however, increases due to more efficient photochemistry paired with increased nighttime minima. Large differences are seen when including the modified exchange coefficients (*enhmix)*, particularly over urban areas at night where turbulent mixing from anthropogenic processes (e.g. traffic) are unaccounted for. Generally, the largest impact is to reduce nighttime ozone titration (i.e., increasing abundances) since the enhancement is only activated under shallow stable boundary layers (< 100 m). Measurements of vertical profiles of various tracer gases are required to conduct more rigorous verification of the new inline PBL mixing in the future. Future work will also investigate adding a

https://doi.org/10.5194/egusphere-2026-4786
Preprint. Discussion started: 13 August 2026

heat flux to the surface layer as an alternate parameterization for both wildfires and anthropogenic activities. Leveraging the urban parametrizations in land surface schemes will also be investigated. The inclusion of the PBL simulated clouds in the TUV scheme reduces photolysis rates leading to 1-5 ppb reductions in surface O_3 across the eastern US (very few PBL clouds are simulated in the west). This coupling is crucial to reduce high ozone bias in air quality models, in particular the regions where shallow convection is prevalent. Overall, we find that improving the coupling between chemistry and physics processes in the experimental RAP-Chem improves its predictions of both weather and atmospheric chemistry.

Code and data availability

The RAP-Chem v1.0 model code, anthropogenic, wildfire, and biogenic emission files, as well as the namelist.wps and Vtable used to generate the initial and lateral boundary conditions are available at 10.5281/zenodo.21793915 (Schnell, 2026) Example namelist.input files for each experiment, all figure plotting scripts or YAML files for MELODIES-MONET, and all model output necessary to reproduce the figures are also included at 10.5281/zenodo.21793915 (Schnell, 2026). The WRF Preprocessing System (WPS) code to generate the initial and lateral boundary conditions is available at https://www2.mmm.ucar.edu/wrf/users/download/get_source.html. The GFS data is available at https://www.nco.ncep.noaa.gov/pmb/products/gfs and RAQMS data is from http://raqms-ops.ssec.wisc.edu/. The MELODIES-MONET platform can be installed via the instructions at https://melodies-monet.readthedocs.io/en/stable/, which also enables efficient download and preprocessing of the NOAA ISD, EPA AirNow, and AERONET observation data used herein. MODIS AQUA AIRS data can be retrieved from https://search.earthdata.nasa.gov/. NOAA GML SURFRAD and SOLRAD data can be retrieved from https://gml.noaa.gov/aftp/data/radiation/.

Author contributions

JS and RA designed the experiments. JS carried out the experiments, performed the data analysis, and led the writing of the paper. JS, RA, GAG, JBO, EJ, MH, BB, SF contributed to the model code. BM, RHS, JH, CH, RBP, MC, GP,, and MT helped generate ancillary input data. All other authors contributed to the writing and review of the manuscript.

Competing interests

The authors declare that they have no conflict of interest.

Disclaimer

The statements, findings, conclusions, and recommendations are those of the author(s) and do not necessarily reflect the views of NOAA or the U.S. Department of Commerce.

https://doi.org/10.5194/egusphere-2026-4786
Preprint. Discussion started: 13 August 2026

Acknowledgments

The authors wish to thank the administrators of the Jet supercomputer in Boulder, CO for their tireless efforts maintaining the computing environment and system. We also acknowledge the usage of Google Gemini in the assistance of the creation of some of the plotting routines.

Financial Support

This research was supported in part by the NOAA cooperative agreement NA22OAR4320151, for the Cooperative Institute for Earth System Research and Data Science (CIESRDS), and the Earth Radiation Budget (ERB) initiative.

References

Ahmadov, R., Grell, G., James, E., Csiszar, I., Tsidulko, M., Pierce, B., McKeen, S., Benjamin, S., Alexander, C., Pereira, G., Freitas, S., Goldberg, M., 2017. Using VIIRS fire radiative power data to simulate biomass burning emissions, plume rise and smoke transport in a real-time air quality modeling system, in: 2017 IEEE International Geoscience and Remote Sensing Symposium (IGARSS). Presented at the 2017 IEEE International Geoscience and Remote Sensing Symposium (IGARSS), IEEE, Fort Worth, TX, pp. 2806–2808. https://doi.org/10.1109/IGARSS.2017.8127581

Ahmadov, R., McKeen, S.A., Robinson, A.L., Bahreini, R., Middlebrook, A.M., De Gouw, J.A., Meagher, J., Hsie, E. -Y., Edgerton, E., Shaw, S., Trainer, M., 2012. A volatility basis set model for summertime secondary organic aerosols over the eastern United States in 2006. J. Geophys. Res. Atmospheres 117, 2011JD016831. https://doi.org/10.1029/2011JD016831

Andreae, M.O., 2019. Emission of trace gases and aerosols from biomass burning – an updated assessment. Atmospheric Chem. Phys. 19, 8523–8546. https://doi.org/10.5194/acp-19-8523-2019

Augustine, J.A., DeLuisi, J.J., Long, C.N., 2000. SURFRAD—A National Surface Radiation Budget Network for Atmospheric Research. Bull. Am. Meteorol. Soc. 81, 2341–2357. https://doi.org/10.1175/1520-0477(2000)081%3C2341:SANSRB%3E2.3.CO;2

Augustine, J.A., Hodges, G.B., Cornwall, C.R., Michalsky, J.J., Medina, C.I., 2005. An Update on SURFRAD—The GCOS Surface Radiation Budget Network for the Continental United States. J. Atmospheric Ocean. Technol. 22, 1460–1472. https://doi.org/10.1175/JTECH1806.1

Benjamin, S.G., Weygandt, S.S., Brown, J.M., Hu, M., Alexander, C.R., Smirnova, T.G., Olson, J.B., James, E.P., Dowell, D.C., Grell, G.A., Lin, H., Peckham, S.E., Smith, T.L., Moninger, W.R., Kenyon, J.S., Manikin, G.S., 2016. A North American Hourly Assimilation and Model Forecast Cycle: The Rapid Refresh. Mon. Weather Rev. 144, 1669–1694. https://doi.org/10.1175/MWR-D-15-0242.1

Bruckner, M., Pierce, R.B., Lenzen, A., Diskin, G., DiGangi, J., De Maziere, M., Jones, N., Makarova, M., 2024. UFS-RAQMS Global Atmospheric Composition Model: TROPOMI CO Column Assimilation. https://doi.org/10.5194/egusphere-2024-2501

Campbell, P.C., Tang, Y., Lee, P., Baker, B., Tong, D., Saylor, R., Stein, A., Huang, J., Huang, H.-C., Strobach, E., McQueen, J., Pan, L., Stajner, I., Sims, J., Tirado-Delgado, J., Jung, Y., Yang, F., Spero, T.L., Gilliam, R.C., 2022. Development and evaluation of an advanced National Air Quality Forecasting Capability using the NOAA Global Forecast System version 16. Geosci. Model Dev. 15, 3281–3313. https://doi.org/10.5194/gmd-15-3281-2022

https://doi.org/10.5194/egusphere-2026-4786
Preprint. Discussion started: 13 August 2026

595 Chow, F.K., Yu, K.A., Young, A., James, E., Grell, G.A., Csiszar, I., Tsidulko, M., Freitas, S., Pereira, G., Giglio, L., Friberg,
596 M.D., Ahmadov, R., 2022. High-Resolution Smoke Forecasting for the 2018 Camp Fire in California. Bull. Am.
597 Meteorol. Soc. 103, E1531–E1552. https://doi.org/10.1175/BAMS-D-20-0329.1
598 Clough, S.A., Shephard, M.W., Mlawer, E.J., Delamere, J.S., Iacono, M.J., Cady-Pereira, K., Boukabara, S., Brown, P.D.,
599 2005. Atmospheric radiative transfer modeling: a summary of the AER codes. J. Quant. Spectrosc. Radiat. Transf.
600 91, 233–244. https://doi.org/10.1016/j.jqsrt.2004.05.058
601 Coggon, M.M., Gkatzelis, G.I., McDonald, B.C., Gilman, J.B., Schwantes, R.H., Abuhassan, N., Aikin, K.C., Arend, M.F.,
602 Berkoff, T.A., Brown, S.S., Campos, T.L., Dickerson, R.R., Gronoff, G., Hurley, J.F., Isaacman-VanWertz, G., Koss,
603 A.R., Li, M., McKeen, S.A., Moshary, F., Peischl, J., Pospisilova, V., Ren, X., Wilson, A., Wu, Y., Trainer, M.,
604 Warneke, C., 2021. Volatile chemical product emissions enhance ozone and modulate urban chemistry. Proc. Natl.
605 Acad. Sci. 118, e2026653118. https://doi.org/10.1073/pnas.2026653118
606 Conrick, R., Mass, C.F., Boomgard-Zagrodnik, J.P., Ovens, D., 2021. The Influence of Wildfire Smoke on Cloud
607 Microphysics during the September 2020 Pacific Northwest Wildfires. Weather Forecast.
608 https://doi.org/10.1175/WAF-D-21-0044.1
609 Dowell, D.C., Alexander, C.R., James, E.P., Weygandt, S.S., Benjamin, S.G., Manikin, G.S., Blake, B.T., Brown, J.M.,
610 Olson, J.B., Hu, M., Smirnova, T.G., Ladwig, T., Kenyon, J.S., Ahmadov, R., Turner, D.D., Duda, J.D., Alcott, T.I.,
611 2022. The High-Resolution Rapid Refresh (HRRR): An Hourly Updating Convection-Allowing Forecast Model.
612 Part I: Motivation and System Description. Weather Forecast. 37, 1371–1395.
613 https://doi.org/10.1175/WAF-D-21-0151.1
614 Fast, J.D., Gustafson, W.I., Easter, R.C., Zaveri, R.A., Barnard, J.C., Chapman, E.G., Grell, G.A., Peckham, S.E., 2006.
615 Evolution of ozone, particulates, and aerosol direct radiative forcing in the vicinity of Houston using a fully coupled
616 meteorology-chemistry-aerosol model. J. Geophys. Res.-Atmospheres 111, 29.
617 https://doi.org/10.1029/2005jd006721
618 Francoeur, C.B., McDonald, B.C., Gilman, J.B., Zarzana, K.J., Dix, B., Brown, S.S., De Gouw, J.A., Frost, G.J., Li, M.,
619 McKeen, S.A., Peischl, J., Pollack, I.B., Ryerson, T.B., Thompson, C., Warneke, C., Trainer, M., 2021. Quantifying
620 Methane and Ozone Precursor Emissions from Oil and Gas Production Regions across the Contiguous US. Environ.
621 Sci. Technol. 55, 9129–9139. https://doi.org/10.1021/acs.est.0c07352
622 Freitas, S.R., Grell, G.A., Li, H., 2021. The Grell–Freitas (GF) convection parameterization: recent developments,
623 extensions, and applications. Geosci. Model Dev. 14, 5393–5411. https://doi.org/10.5194/gmd-14-5393-2021
624 Gery, M.W., Whitten, G.Z., Killus, J.P., Dodge, M.C., 1989. A photochemical kinetics mechanism for urban and regional
625 scale computer modeling. J. Geophys. Res. Atmospheres 94, 12925–12956.
626 https://doi.org/10.1029/JD094iD10p12925
627 Grell, G.A., Dévényi, D., 2002. A generalized approach to parameterizing convection combining ensemble and data
628 assimilation techniques. Geophys. Res. Lett. 29. https://doi.org/10.1029/2002GL015311
629 Grell, G.A., Freitas, S.R., 2014. A scale and aerosol aware stochastic convective parameterization for weather and air quality
630 modeling. Atmospheric Chem. Phys. 14, 5233–5250. https://doi.org/10.5194/acp-14-5233-2014
631 Grell, G.A., Peckham, S.E., Schmitz, R., McKeen, S.A., Frost, G., Skamarock, W.C., Eder, B., 2005. Fully coupled "online"
632 chemistry within the WRF model. Atmos. Environ. 39, 6957–6975. https://doi.org/10.1016/j.atmosenv.2005.04.027
633 Guo, J.J., Fiore, A.M., Murray, L.T., Jaffe, D.A., Schnell, J.L., Moore, C.T., Milly, G.P., 2018. Average versus high surface
634 ozone levels over the continental USA: model bias, background influences, and interannual variability. Atmospheric
635 Chem. Phys. 18, 12123–12140. https://doi.org/10.5194/acp-18-12123-2018
636 He, J., Harkins, C., O'Dell, K., Li, M., Francoeur, C., Aikin, K.C., Anenberg, S., Baker, B., Brown, S.S., Coggon, M.M.,
637 Frost, G.J., Gilman, J.B., Kondragunta, S., Lamplugh, A., Lyu, C., Moon, Z., Pierce, B.R., Schwantes, R.H.,
638 Stockwell, C.E., Warneke, C., Yang, K., Nowlan, C.R., González Abad, G., McDonald, B.C., 2023. COVID-19
639 perturbation on US air quality and human health impact assessment. PNAS Nexus 3, pgad483.
640 https://doi.org/10.1093/pnasnexus/pgad483
641 Higuera, P.E., Abatzoglou, J.T., 2021. Record-setting climate enabled the extraordinary 2020 fire season in the western
642 United States. Glob. Change Biol. 27, 1–2. https://doi.org/10.1111/gcb.15388

https://doi.org/10.5194/egusphere-2026-4786
Preprint. Discussion started: 13 August 2026

Holben, B.N., Eck, T.F., Slutsker, I., Tanré, D., Buis, J.P., Setzer, A., Vermote, E., Reagan, J.A., Kaufman, Y.J., Nakajima, T., Lavenu, F., Jankowiak, I., Smirnov, A., 1998. AERONET—A Federated Instrument Network and Data Archive for Aerosol Characterization. Remote Sens. Environ. 66, 1–16. https://doi.org/10.1016/S0034-4257(98)00031-5

Holben, B.N., Tanré, D., Smirnov, A., Eck, T.F., Slutsker, I., Abuhassan, N., Newcomb, W.W., Schafer, J.S., Chatenet, B., Lavenu, F., Kaufman, Y.J., Castle, J.V., Setzer, A., Markham, B., Clark, D., Frouin, R., Halthore, R., Karneli, A., O'Neill, N.T., Pietras, C., Pinker, R.T., Voss, K., Zibordi, G., 2001. An emerging ground-based aerosol climatology: Aerosol optical depth from AERONET. J. Geophys. Res. Atmospheres 106, 12067–12097. https://doi.org/10.1029/2001JD900014

Houweling, S., Dentener, F., Lelieveld, J., 1998. The impact of nonmethane hydrocarbon compounds on tropospheric photochemistry. J. Geophys. Res. Atmospheres 103, 10673–10696. https://doi.org/10.1029/97JD03582

Hu, X.-M., Doughty, D.C., Sanchez, K.J., Joseph, E., Fuentes, J.D., 2012. Ozone variability in the atmospheric boundary layer in Maryland and its implications for vertical transport model. Atmos. Environ. 46, 354–364. https://doi.org/10.1016/j.atmosenv.2011.09.054

James, E.P., Alexander, C.R., Dowell, D.C., Weygandt, S.S., Benjamin, S.G., Manikin, G.S., Brown, J.M., Olson, J.B., Hu, M., Smirnova, T.G., Ladwig, T., Kenyon, J.S., Turner, D.D., 2022. The High-Resolution Rapid Refresh (HRRR): An Hourly Updating Convection-Allowing Forecast Model. Part II: Forecast Performance. Weather Forecast. 37, 1397–1417. https://doi.org/10.1175/WAF-D-21-0130.1

Li, H., Grell, G.A., Ahmadov, R., Zhang, L., Sun, S., Schnell, J., Wang, N., 2024. A simple and realistic aerosol emission approach for use in the Thompson–Eidhammer microphysics scheme in the NOAA UFS Weather Model (version GSL global-24Feb2022). Geosci. Model Dev. 17, 607–619. https://doi.org/10.5194/gmd-17-607-2024

Li, Y., Pickering, K.E., Barth, M.C., Bela, M.M., Cummings, K.A., Allen, D.J., 2019. Wet Scavenging in WRF-Chem Simulations of Parameterized Convection for a Severe Storm During the DC3 Field Campaign. J. Geophys. Res. Atmospheres 124, 7413–7428. https://doi.org/10.1029/2019JD030484

Li, Y., Pickering, K.E., Barth, M.C., Bela, M.M., Cummings, K.A., Allen, D.J., 2018. Evaluation of Parameterized Convective Transport of Trace Gases in Simulation of Storms Observed During the DC3 Field Campaign. J. Geophys. Res. Atmospheres 123. https://doi.org/10.1029/2018JD028779

Lin, Y.-L., Farley, R.D., Orville, H.D., 1983. Bulk Parameterization of the Snow Field in a Cloud Model. J. Clim. Appl. Meteorol. 22, 1065–1092. https://doi.org/10.1175/1520-0450(1983)022%3C1065:BPOTSF%3E2.0.CO;2

Madronich, S., Flocke, S., 1997. Theoretical Estimation of Biologically Effective UV Radiation at the Earth's Surface, in: Zerefos, C.S., Bais, A.F. (Eds.), Solar Ultraviolet Radiation. Springer Berlin Heidelberg, Berlin, Heidelberg, pp. 23–48. https://doi.org/10.1007/978-3-662-03375-3_3

Malm, W.C., Sisler, J.F., Huffman, D., Eldred, R.A., Cahill, T.A., 1994. Spatial and seasonal trends in particle concentration and optical extinction in the United States. J. Geophys. Res. Atmospheres 99, 1347–1370. https://doi.org/10.1029/93JD02916

McDonald, B.C., De Gouw, J.A., Gilman, J.B., Jathar, S.H., Akherati, A., Cappa, C.D., Jimenez, J.L., Lee-Taylor, J., Hayes, P.L., McKeen, S.A., Cui, Y.Y., Kim, S.-W., Gentner, D.R., Isaacman-VanWertz, G., Goldstein, A.H., Harley, R.A., Frost, G.J., Roberts, J.M., Ryerson, T.B., Trainer, M., 2018. Volatile chemical products emerging as largest petrochemical source of urban organic emissions. Science 359, 760–764. https://doi.org/10.1126/science.aaq0524

McDuffie, E.E., Smith, S.J., O'Rourke, P., Tibrewal, K., Venkataraman, C., Marais, E.A., Zheng, B., Crippa, M., Brauer, M., Martin, R.V., 2020. A global anthropogenic emission inventory of atmospheric pollutants from sector- and fuel-specific sources (1970–2017): an application of the Community Emissions Data System (CEDS). Earth Syst. Sci. Data 12, 3413–3442. https://doi.org/10.5194/essd-12-3413-2020

Morrison, H., Curry, J.A., Khvorostyanov, V.I., 2005. A New Double-Moment Microphysics Parameterization for Application in Cloud and Climate Models. Part I: Description. J. Atmospheric Sci. 62, 1665–1677. https://doi.org/10.1175/JAS3446.1

Nakanishi, M., Niino, H., 2009. Development of an Improved Turbulence Closure Model for the Atmospheric Boundary Layer. J. Meteorol. Soc. Jpn. Ser II 87, 895–912. https://doi.org/10.2151/jmsj.87.895

Nakanishi, M., Niino, H., 2004. An Improved Mellor–Yamada Level-3 Model with Condensation Physics: Its Design and Verification. Bound.-Layer Meteorol. 112, 1–31. https://doi.org/10.1023/B:BOUN.0000020164.04146.98

https://doi.org/10.5194/egusphere-2026-4786
Preprint. Discussion started: 13 August 2026

Olson, J., Angevine, W.M., Turner, D.D., Sun, X., Simonson, J.M., Evans, C., Kenyon, J.S., Li, H., Schnell, J., Puhales, F.S., Cherubini, T., Li, W., Zhang, M., 2026. A Description of the MYNN-EDMF Turbulence Scheme. NOAA Tech. Memo. OAR GSL 77. https://doi.org/10.25923/RAHR-SJ70

Pleim, J.E., 2007. A Combined Local and Nonlocal Closure Model for the Atmospheric Boundary Layer. Part I: Model Description and Testing. J. Appl. Meteorol. Climatol. 46, 1383–1395. https://doi.org/10.1175/JAM2539.1

Powers, J.G., Klemp, J.B., Skamarock, W.C., Davis, C.A., Dudhia, J., Gill, D.O., Coen, J.L., Gochis, D.J., Ahmadov, R., Peckham, S.E., Grell, G.A., Michalakes, J., Trahan, S., Benjamin, S.G., Alexander, C.R., Dimego, G.J., Wang, W., Schwartz, C.S., Romine, G.S., Liu, Z.Q., Snyder, C., Chen, F., Barlage, M.J., Yu, W., Duda, M.G., 2017. THE WEATHER RESEARCH AND FORECASTING MODEL Overview, System Efforts, and Future Directions. Bull. Am. Meteorol. Soc. 98, 1717–1737. https://doi.org/10.1175/bams-d-15-00308.1

Schnell, J., 2026. Supporting data for Schnell et al., "Tight physics and chemistry coupling improves air quality forecasts: a case study of the 2020 North American wildfires with the Rapid Refresh model coupled to Chemistry (RAP-Chem v1.0)." https://doi.org/10.5281/ZENODO.20667784

Schwantes, R.H., Emmons, L.K., Orlando, J.J., Barth, M.C., Tyndall, G.S., Hall, S.R., Ullmann, K., St. Clair, J.M., Blake, D.R., Wisthaler, A., Bui, T.P.V., 2020. Comprehensive isoprene and terpene gas-phase chemistry improves simulated surface ozone in the southeastern US. Atmospheric Chem. Phys. 20, 3739–3776. https://doi.org/10.5194/acp-20-3739-2020

Skamarock, W., Klemp, J., Dudhia, J., Gill, D., Barker, D., Wang, W., Huang, X.-Y., Duda, M., 2008. A Description of the Advanced Research WRF Version 3. UCAR/NCAR. https://doi.org/10.5065/D68S4MVH

Smirnova, T.G., Brown, J.M., Benjamin, S.G., Kenyon, J.S., 2016. Modifications to the Rapid Update Cycle Land Surface Model (RUC LSM) Available in the Weather Research and Forecasting (WRF) Model. Mon. Weather Rev. 144, 1851–1865. https://doi.org/10.1175/MWR-D-15-0198.1

Stockwell, C.E., Coggon, M.M., Gkatzelis, G.I., Ortega, J., McDonald, B.C., Peischl, J., Aikin, K., Gilman, J.B., Trainer, M., Warneke, C., 2021. Volatile organic compound emissions from solvent- and water-borne coatings – compositional differences and tracer compound identifications. Atmospheric Chem. Phys. 21, 6005–6022. https://doi.org/10.5194/acp-21-6005-2021

Tang, W., Emmons, L.K., Buchholz, R.R., Wiedinmyer, C., Schwantes, R.H., He, C., Kumar, R., Pfister, G.G., Worden, H.M., Hornbrook, R.S., Apel, E.C., Tilmes, S., Gaubert, B., Martinez-Alonso, S., Lacey, F., Holmes, C.D., Diskin, G.S., Bourgeois, I., Peischl, J., Ryerson, T.B., Hair, J.W., Weinheimer, A.J., Montzka, D.D., Tyndall, G.S., Campos, T.L., 2022. Effects of Fire Diurnal Variation and Plume Rise on U.S. Air Quality During FIREX-AQ and WE-CAN Based on the Multi-Scale Infrastructure for Chemistry and Aerosols (MUSICAv0). J. Geophys. Res. Atmospheres 127, e2022JD036650. https://doi.org/10.1029/2022JD036650

Thompson, G., Eidhammer, T., 2014. A Study of Aerosol Impacts on Clouds and Precipitation Development in a Large Winter Cyclone. J. Atmospheric Sci. 71, 3636–3658. https://doi.org/10.1175/jas-d-13-0305.1

Wozniak, M.C., Steiner, A.L., 2017. A prognostic pollen emissions model for climate models (PECM1.0). Geosci. Model Dev. 10, 4105–4127. https://doi.org/10.5194/gmd-10-4105-2017

Zhou, X., Josey, K., Kamareddine, L., Caine, M.C., Liu, T., Mickley, L.J., Cooper, M., Dominici, F., 2021. Excess of COVID-19 cases and deaths due to fine particulate matter exposure during the 2020 wildfires in the United States. Sci. Adv. 7, eabi8789. https://doi.org/10.1126/sciadv.abi8789